

Experimental Observations and Numerical Modeling of Coupled Microbial and Transport Processes in Variably Saturated Sand

M. L. Rockhold,* R. R. Yarwood, M. R. Niemet, P. J. Bottomley, and J. S. Selker

ABSTRACT

An experimental and numerical investigation was conducted to study interactions between microbial dynamics and transport processes in variably saturated porous media. Experiments were conducted with constant, surface-applied water fluxes in duplicate, variably saturated, sand-filled columns that were uniformly inoculated with the bacterium *Pseudomonas fluorescens* HK44. The permeability of the sand in the columns was reduced by a factor of 45 during 1 wk of growth on glucose. Pressure heads increased (became less negative) at all measured depths, but significant increases in the apparent volumetric water contents were observed in only the upper 5 cm of the columns, corresponding to the areas with the highest concentrations of attached bacteria. A numerical model was used to simulate the experiments. The model accounted for the processes of water flow, solute and bacterial transport, cell growth and accumulation, glucose and O₂ consumption, and gas diffusion and exchange. Observed changes in water content and pressure head were reproduced approximately using fluid-media scaling to account for an apparent surface-tension lowering effect. Reasonable correspondence was obtained between observed and simulated effluent data and final attached biomass concentration distributions using first-order reversible cell attachment and detachment kinetics. The attachment rate coefficients were based on particle-filtration theory and time-dependent detachment rate coefficients. The results of this study illustrate the potential importance of using fully coupled multifluid flow and multicomponent reactive transport equations to model coupled biogeochemical and transport processes in soils.

A SIGNIFICANT BODY OF RESEARCH exists on the transport and biodegradation of various contaminants in saturated porous media systems that are representative of aquifer materials. Comparatively little work has been done to study biodegradation or bioremediation on a mechanistic basis in more complicated unsaturated porous media systems such as soils. Several studies have been conducted on the transport of bacteria in soils or unsaturated porous media under nongrowth conditions (Tan et al., 1992; Wan et al., 1994; Schäfer et al., 1998; Powelson and Mills, 1998; Jewett et al., 1999). A number of studies have also been conducted on the transport and degradation of model contaminants in soils (Estrella et al., 1993; Allen-King et al. (1996a, 1996b); Langner et al., 1998). However, the majority of the studies on

contaminant transport and degradation in soils have represented biodegradation as a first-order decay process, without actually considering microbial processes and their interactions with other transport processes (Rockhold et al., 2004).

In the work of Estrella et al. (1993), the transport and fate of 2,4-dichloro-phenoxyacetic acid (2,4-D) was studied in both saturated and unsaturated soils. They determined that sorption had a slight but significant effect on 2,4-D transport, but that biodegradation was extensive, under both saturated and unsaturated conditions, following a lag period of up to 3 d. One of their most significant findings was that degradation rate parameters determined from batch experiments were significantly different from those determined in column experiments. The differences were attributed, in part, to possible O₂ limitations in their saturated experiments that were either not present or less severe in their unsaturated experiments. Their column experiments were conducted under steady flow conditions, in both saturated and unsaturated soil, and they modeled these experiments using analytical and numerical models for aqueous phase transport of 2,4-D only. Other processes such as O₂ transport in the aqueous and gas phases, interphase exchange, O₂-limited 2,4-D degradation kinetics, and bacterial growth were not considered.

Langner et al. (1998) studied 2,4-D transport and degradation in batch and unsaturated column experiments with columns of different lengths. They determined that a single set of independently determined rate parameters from batch experiments could not describe 2,4-D degradation for all transport conditions. Apparent first-order degradation rate constants obtained from column data were found to be independent of column residence time, but increased with decreasing pore water velocity, especially at low velocities. They speculated that variations in apparent degradation rates were due to changes in microbial attachment and distribution under different flow rates, differences in the residence time or “local opportunity” time for degradation, or differences in nutrient desorption rates from the solid phase at different pore water velocities. They stated that there is a “need to develop a better understanding of coupled processes involving contaminant degradation and transport.”

The general objective of our work was to gain a better understanding of possible interactions and feedback mechanisms between bacterial growth, water flow, solute transport, and gas exchange in soils. These interactions have important consequences for applications such as

M.L. Rockhold, Pacific Northwest National Lab., P.O. Box 999/MSIN K9-36, Richland, WA 99352; R.R. Yarwood, Dep. of Crop and Soil Sciences, Oregon State Univ., Corvallis, OR 97331; M.R. Niemet, CH2M Hill, 2300 NW Walnut Blvd., Corvallis, OR 97330; P.J. Bottomley, Dep. of Microbiology, Nash Hall, Oregon State Univ., Corvallis, OR 97331; J.S. Selker, Dep. of Bioengineering, Oregon State Univ., Corvallis, OR 97331. Received 16 June 2004. Original Research Paper. *Corresponding author (mark.rockhold@pnl.gov).

Published in Vadose Zone Journal 4:407–417 (2005).

doi:10.2136/vzj2004.0087

© Soil Science Society of America

677 S. Segoe Rd., Madison, WI 53711 USA

Abbreviations: DO, dissolved oxygen; EM, electromagnetic; MMS, minimal mineral salts; TDR, time domain reflectometry; UV, ultraviolet; 2,4-D, 2,4-dichloro-phenoxyacetic acid.

water and wastewater treatment or bioremediation of contaminated soils and aquifer sediments, as well as being of general ecological interest. Specific objectives of this study were to (i) quantify the impact of bacterial growth on the hydraulic properties of variably saturated sand and (ii) develop a numerical model to simulate these processes.

MATERIALS AND METHODS

Instrumentation

Duplicate, segmented, 7.62-cm-diameter (3 in. o.d.) acrylic columns were used in the experiments. The segments were machined in two heights, 1.8 and 6.0 cm, with finished inside diameters of 4.28 cm. The shorter segments were used in the upper, unsaturated part of the columns to provide higher spatial resolution in this region. A brass screen 0.149 mm (100 mesh) was placed in the bottom end-cap to retain the porous media. A relatively coarse screen was used instead of a finer, porous ceramic disc or stainless-steel plate, on which a negative pressure could be applied, to avoid clogging by bacterial cell aggregates or biofilms. The effluent lines were split so that samples could be collected periodically from one end for measurement of dissolved oxygen (DO). The other end was used for effluent outflow and head control. The column segments were held together with three threaded stainless-steel rods. The total height of the columns in which sand could be packed was approximately 55 cm. Experiments were conducted with sand packed to a height of 48 cm to allow room for drip emitters on the tops of the columns. The experimental setup is depicted in Fig. 1.

Alternating smaller segments in the columns were machined with inner water chambers and porous ceramic ring inserts, sealed in place with epoxy, to form tensiometers. The

ceramic rings were cut from larger cylindrical ceramic tubes (Osmonics, Inc., Minnetonka, MN) with a nominal pore diameter of 10 μm , corresponding to a bubbling pressure of approximately 300 cm. Pressure transducers (Honeywell Micro Switch model 26PCBFA1G) were fitted to the tensiometers and were excited and monitored by a personal computer (PC) with a 12-bit data acquisition card (AT-MIO-64E-3), controlled by LabVIEW software (National Instruments Corp., Austin, TX).

The other set of the alternating smaller column segments and two of the larger segments in each column were machined and fitted with miniature, two-wire, time-domain-reflectometry (TDR) probes. The TDR probes were made from 0.9-mm-diameter stainless-steel wire plated with 14K gold to facilitate soldering to commercially available SMA bulkhead connectors (ITT Type 50-645-4524-310). The TDR probes were connected to a Tektronix Model 11801 digital sampling oscilloscope with an SD-24 sampling head (Tektronix, Beaverton, OR). The 20-GHz oscilloscope generates a step electromagnetic pulse with a rise time of 25 ps at the connector on the instrument (Kelly et al., 1995). The TDR signals were transferred from the oscilloscope to a PC via a general purpose interface bus that was controlled by a custom developed Microsoft Excel spreadsheet macro (VBA program). The spreadsheet program automatically plotted TDR waveforms and computed travel times. Apparent liquid saturations were calculated from travel times using regression equations established in independent calibration experiments.

Steady unsaturated fluxes of an autoclaved minimal mineral salts (MMS) solution containing 250 mg L^{-1} of glucose were applied to the upper surfaces of the columns through cylindrical acrylic manifolds that were each fitted with seven 16-gauge hypodermic needles (Fig. 1). Randomized drips were emitted from the needles over the exposed upper surface area of the porous media in each column. The manifolds were connected

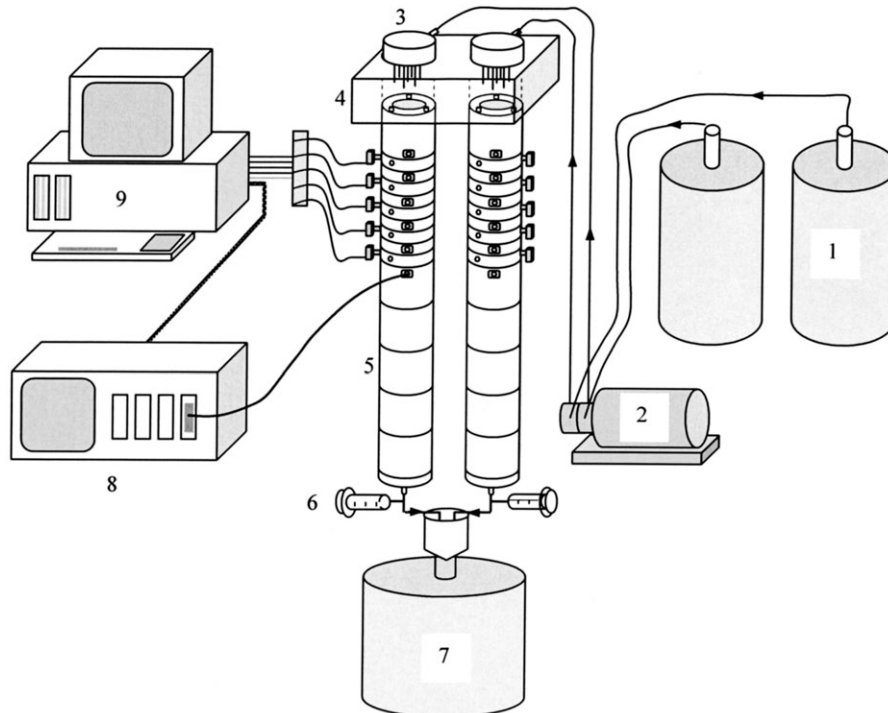


Fig. 1. Setup for column experiments. Components include: carboys containing aqueous influent solutions of minimal mineral salts and glucose (1); peristaltic pump (2), drip emitters (3); housing containing ultraviolet lights (4); segmented, 55-cm-long acrylic columns with ring tensiometers, pressure transducers, and TDR probes (5); syringes for dissolved oxygen sampling (6); carboy for collection of waste effluent (7); Tektronix Model 11801 digital sampling oscilloscope (8); and computer with data acquisition board (9).

to a peristaltic pump using food grade, autoclavable tubing (06402-13, Cole-Parmer, Vernon Hills, IL).

The drip emitters were mounted on top of a vented, foil-lined acrylic box in which two 254-nm-wavelength, ultraviolet (UV) germicidal lamps were housed. The box was attached to the tops of the columns as depicted in Fig. 1. The UV lamps were activated on regular intervals to maintain the sterility of the sand and drippers at the surface of the columns. Auxiliary experiments indicated that the UV light only penetrated the sand a distance equivalent to a few grains or less, so it only sterilized the upper surfaces of the sand in the columns and did not impact biomass growth elsewhere within sand pack.

Effluent samples were collected periodically during the experiments to measure DO using a YSI model 5300 biological oxygen meter with a model 5331 oxygen electrode (Yellow Springs Instrument Company, Yellow Springs, OH). Effluent samples were transferred via syringe from the effluent lines to a sampling chamber within a constant temperature water bath that housed the DO electrode.

Bacteria, Porous Media, and Column Setup

The bacterium used in this study was *Pseudomonas fluorescens* HK44, hereafter referred to as HK44. This bacterium is a gram-negative, rod-shaped, motile bacterium that was originally isolated from soil samples that were collected from a naphthalene contaminated field site. HK44 has been genetically engineered so that it generates bioluminescence in the presence of naphthalene or its metabolite salicylate (King et al., 1990). This bioluminescence was utilized by Yarwood et al. (2002) for nondestructive quantification of cell density and distribution in a two-dimensional, light transmission chamber containing unsaturated porous media. On average, a fully hydrated HK44 cell is approximately 2.4 by 0.8 μm , with a dry cell weight of about 2.7×10^{-10} mg, and with 55% of this dry cell weight consisting of protein (Yarwood et al., 2002). The average density of a fully hydrated cell was assumed to be 1100 mg cm^{-3} (Bouwer and Rittmann, 1992). HK44 was grown overnight in the MMS medium, supplemented with 1 g L^{-1} glucose, and then resuspended in the basal MMS medium before use in the column experiments (Yarwood et al., 2002).

The porous media used in the experiments was a 40/50 grade of quartz Accusand (Unimin Co., LeSueur, MN). Physical properties and chemical analyses of several grades of Accusand were described by Schroth et al. (1996). The reported median grain diameter (d_{50}), uniformity coefficient (d_{60}/d_{10}), and particle sphericity of the 40/50 grade are 0.359 ± 0.01 mm, 1.2 ± 0.018 , and 0.9, respectively. The cation-exchange capacity, total Fe content, Fe oxide content, and organic C content are reported to be $0.67 \text{ cmol kg}^{-1}$, 5.58 g kg^{-1} , 0.3 g kg^{-1} , and 0.3 g kg^{-1} , respectively. Before packing, the sand was soaked in a 5 M NaCl solution followed by thorough rinsing in distilled water to remove fine particulates. The damp sand was then autoclaved three times, for 1 h each time, and allowed to stand at room temperature for at least 24 h between each autoclaving for sterilization.

The columns were sterilized by submerging them for approximately 10 min in a 0.8 M (5%) sodium hypochlorite (bleach) solution, followed by thorough rinsing with sterile, deionized water. The tensiometer segments were rinsed and refilled with sterile, deaired water. The barrels of the pressure transducers were rinsed with an 18 M (70%) ethanol solution, followed by thorough rinsing with sterile deionized water. The deionized water was then displaced with sterile, deaired water using a sterile syringe and hypodermic needle, before attaching them to the tensiometer segments, to ensure that no air bubbles were trapped in the barrels of the transducers.

The columns were wet-packed by first filling them with approximately 300 mL of an otherwise sterile MMS solution containing approximately $5 \times 10^8 \text{ CFU mL}^{-1}$ of HK44. Dry, autoclaved 40/50 Accusand was then poured into the tops of the columns through a sterile funnel. The columns were gently tapped with a rubber mallet while the sand was continuously poured until a maximum packing height of 48 cm was reached. The wet packing procedure ensured that the sand in the columns was fully saturated with no apparent entrapped air.

After the columns were packed, the UV light box and dripper manifolds were mounted on the tops of the columns, and the UV light box was turned on to sterilize the upper ends of the columns. Initial TDR and pressure transducer readings were collected. A steady flux of 250 mg L^{-1} of glucose in MMS solution was then started on the tops of the columns at a flow rate of 7 cm h^{-1} while the columns were still fully saturated. The outflow lines were partially opened, and the outflow rate was adjusted during the initial stages of drainage so that it was only slightly greater than the inflow rate, in an attempt to minimize the effects of hysteresis and air entrapment. The outflow lines were opened completely after about 20 min. The ends of the outflow lines were positioned so that zero pressure was established 1 cm above the retaining screen at the base of the columns.

Effluent samples were collected periodically to measure concentrations of glucose and aqueous-phase bacteria. Samples were also extracted periodically from sampling lines at the base of the columns for measurement of DO. Aqueous-phase cell concentrations were determined by measuring protein using bicinchoninic acid (Smith et al., 1985) with a Micro BCA Protein Assay Reagent Kit (Pierce, Rockford, IL). Correlations between protein and cell concentration were established by plate count. Glucose concentrations were determined using anthrone (Brink et al., 1960).

Model Description

Water flow was modeled using the Richards (1931) equation:

$$\frac{\partial(\phi S_w)}{\partial t} = \frac{\partial}{\partial z} \left[K_z k_r \left(\frac{\partial h}{\partial z} + 1 \right) \right] \pm \Omega \quad [1]$$

where ϕ is the porosity, S_w is the aqueous-phase saturation, t is time, z is the vertical coordinate, K_z is the saturated hydraulic conductivity, k_r is the relative hydraulic conductivity, h is the soil water pressure head, and Ω is a volumetric flux due to liquid sources or sinks.

A fixed head (Dirichlet) boundary condition was applied to the lower boundary:

$$h(z, t) = h_0(t); z = L \quad [2]$$

and a prescribed flux (Neumann) boundary was specified for the upper boundary:

$$-K \frac{\partial h}{\partial z} + 1 = q_{w0}(z, t); z = 0 \quad [3]$$

where h_0 and q_{w0} are the prescribed pressure head and water flux, respectively.

Solute and bacterial transport, cell growth, substrate consumption, and gas diffusion were modeled using advection-dispersion reaction equations of the form:

$$\frac{\partial}{\partial t} (R_f \theta_\ell C_{k,\ell}) = \frac{\partial}{\partial z} \left[\theta_\ell D_{k,\ell} \left(\frac{\partial C_{k,\ell}}{\partial z} \right) \right] - \frac{\partial}{\partial z} (q_{k,\ell} C_{k,\ell}) + \Lambda_{k,\ell} \quad [4]$$

where R_f is a dimensionless retardation coefficient, θ is the volumetric fluid content, C is the mass of a particular constit-

uent per volume of pore fluid, D is a hydrodynamic dispersion coefficient, q is the Darcian flux, and Λ represents a reaction-rate source-sink term. Subscript k refers to different constituents (e.g., $k = \text{"g"}$ for glucose, O_2 , CO_2 , or "m" for microbes), and subscript ℓ refers to the phase (e.g., $\ell = \text{"w"}$ for water and "a" for air).

For aqueous phase solutes, the hydrodynamic dispersion coefficient was defined as

$$D_{k,w} = \alpha_L |v_w| + D_{k,w}^{\text{eff}} \quad [5]$$

where α_L is the dispersivity, v_w is the water velocity (q/θ), $D_{k,w}^{\text{eff}}$ is the effective molecular diffusion coefficient in water. For O_2 and CO_2 , which partition between the aqueous and gas phases, dispersion in the gas phase was neglected and effective values of the retardation factor, dispersion coefficient, and Darcian flux were defined in a manner analogous to that used by Šimunek and Suarez (1993):

$$R_f = 1 + \left(\frac{M_w}{K_H R T} \right) \left(\frac{\theta_a}{\theta_w} \right) \quad [6]$$

$$\theta_w D_E = \theta_w D_{k,w} + \left(\frac{M_w}{K_H R T} \right) \theta_a D_{k,a}^{\text{eff}} \quad [7]$$

$$q_E = q_w + \left(\frac{M_w}{K_H R T} \right) q_a \quad [8]$$

where M_w is the molecular weight, K_H is the Henry's Law constant, R is the ideal gas constant, and T is absolute temperature. Effective diffusion coefficients were defined as

$$D_{k,\ell}^{\text{eff}} = D_{k,\ell}^{\text{mol}} \left(\frac{\theta_\ell^e}{\phi^e} \right) \quad [9]$$

where a and e are empirical parameters (Millington and Quirk, 1961; Moldrup et al., 2000). Assuming no gas flow across the lower boundary of the columns, the flux of air into or out of the top of the columns during a time step was calculated from

$$q_a(0) = - \int_{z=0}^L \frac{V}{A} \frac{d\theta_w}{dt} dz \quad [10]$$

where V is the volume of porous media represented by a model grid block, and A is the cross-sectional area of the grid block normal to the direction of flow. Vertical air fluxes at other locations were estimated in the same manner.

Boundary conditions for Eq. [4] were handled in a manner similar to that described by Šimunek and Suarez (1993). For the upper boundary, first- or third-type boundary conditions were used

$$C_{k,\ell}(0,t) = C_{k,\ell 0} \quad [11]$$

$$-\theta_w D_E \frac{\partial C_{k,\ell}}{\partial z} + q_E C_{k,\ell} = q_{E0} C_{k,\ell 0} \quad [12]$$

where q_{E0} is the effective flux, and $C_{k,\ell 0}$ is the concentration associated with this flux or prescribed at the boundary. For constituents that exist only in the aqueous phase or partition only between the aqueous and solid phases, the third-type boundary condition was used, and D_E and q_E did not account for the gas phase. For constituents that partition between the aqueous and gas phases, Eq. [6] through [8] define the effective values of R_f , D_E , and q_E , which were used in Eq. [4]. The third-type boundary condition given by Eq. [12] was used for multiphase constituents whenever $q_E > 0$, and the first-type boundary condition given by Eq. [11] was used when $q_E \leq 0$. In both cases, $C_{k,\ell 0} = C_{k,w 0}$, which corresponds to the equilibrium

concentration in the aqueous phase determined by the atmospheric concentration of the gas using Henry's Law. For the lower boundary, a continuous concentration boundary condition was specified:

$$\frac{\partial C_{k,\ell}}{\partial z}(L,t) = 0 \quad [13]$$

The coefficients of molecular diffusion for O_2 and CO_2 in air were estimated from (Jaynes and Rogowski, 1983):

$$D_{\text{O}_2,\text{a}}^{\text{mol}} = \frac{D_{\text{O}_2,\text{CO}_2} D_{\text{O}_2,\text{N}_2}}{D_{\text{O}_2,\text{N}_2} X_{\text{CO}_2} + D_{\text{O}_2,\text{CO}_2} X_{\text{N}_2} + r D_{\text{O}_2,\text{N}_2} X_{\text{O}_2}} \quad [14]$$

$$D_{\text{CO}_2,\text{a}}^{\text{mol}} = \frac{D_{\text{O}_2,\text{CO}_2} D_{\text{CO}_2,\text{N}_2}}{D_{\text{CO}_2,\text{N}_2} X_{\text{O}_2} + D_{\text{O}_2,\text{CO}_2} X_{\text{N}_2} + (D_{\text{CO}_2,\text{N}_2} X_{\text{CO}_2}/r)} \quad [15]$$

where the terms containing D on the right sides of Eq. [14] and Eq. [15] are binary diffusion coefficients for each gas pair, which are assumed to be independent of composition. The terms X_{O_2} , X_{CO_2} , X_{N_2} are the mole fractions of each gas, and r is the respiration coefficient or quotient (moles CO_2 produced per mole O_2 consumed). For consistency with the isobaric assumption, which is implied by the use of the Richards equation, it was assumed that $X_{\text{O}_2} + X_{\text{CO}_2} + X_{\text{N}_2} = 1$. Values of X_{N_2} were updated at the end of each time step, after calculating X_{O_2} and X_{CO_2} , for use in Eq. [14] and [15].

Reactions were assumed to occur only in the aqueous phase and were represented using the following equations:

$$\Lambda_{g,w} = -\mu Y_{g/m} (\theta_w C_{m,w} + \rho_b C_{m,s1}) \quad [16]$$

$$\Lambda_{o,w} = -\mu Y_{o/m} (\theta_w C_{m,w} + \rho_b C_{m,s1}) \quad [17]$$

$$\Lambda_{m,w} = \mu \theta_w C_{m,w} - k_1 \theta_w C_{m,w} + k_2 \rho_b C_{m,s1} \quad [18]$$

where μ is the specific growth rate of the bacterium; $Y_{g/m}$ and $Y_{o/m}$ are yield coefficients representing the mass of electron donor or substrate (e.g., glucose) consumed and the mass of terminal electron acceptor (e.g., O_2) consumed, respectively, per mass of cells generated; k_1 and k_2 are first-order reversible attachment and detachment coefficients, respectively; and ρ_b is the bulk density. The terms $C_{m,w}$ and $C_{m,s1}$ represent the mass of cells in the aqueous phase per volume of pore liquid, and the mass of cells reversibly attached to solids per mass of porous media, respectively.

The specific growth rate was represented by a multiplicative Monod-type kinetics model (McGee et al., 1970):

$$\mu = \mu_{\text{max}} \left(\frac{C_{o,w}}{K_o + C_{o,w}} \right) \left(\frac{C_{g,w}}{K_g + C_{g,w}} \right) \quad [19]$$

where μ_{max} is the maximum specific growth rate (h^{-1}), and K_o and K_g are half-velocity (or half-saturation) coefficients (mg L^{-1}) for O_2 and the glucose, respectively.

The mass balance equation for the attached biomass was

$$\frac{\partial}{\partial t} (\rho_b C_{m,s1}) = \mu \rho_b C_{m,s1} + k_1 \theta_w C_{m,w} - k_2 \rho_b C_{m,s1} \quad [20]$$

where the attachment coefficient, k_1 , was estimated from (Tien et al., 1979)

$$k_1 = \frac{3}{2} \left(\frac{q}{\theta_w} \right) \frac{(1 - \theta_w)}{d_g} \eta \alpha_c \quad [21]$$

where d_g is the median grain diameter of the porous medium (or collector), and η and α_c are the so-called collector and collision (or sticking) efficiencies (Logan et al., 1995; Deshpande and Shonnard, 1999). The η parameter was calculated using the particle-filtration model of Rajagopalan and Tien

(1976). Cell attachment–detachment kinetics were assumed to be related to local environmental conditions, including the presence of growth substrate. The detachment coefficient, k_2 , was represented by

$$k_2 = f \exp(-t_c g_c) \quad [22]$$

where f and g_c are empirical parameters, and t_c was taken as the time since any location in the modeled domain was first exposed to a minimum threshold concentration of growth substrate ($1 \mu\text{g L}^{-1}$ glucose). Although the form of Eq. [22] is somewhat arbitrary, it was found to adequately reproduce the observed behavior of the effluent biomass. Time-dependent attachment–detachment kinetics have been applied previously to model virus and protein adsorption (Lee et al., 1999). Alternative approaches for modeling cell attachment and detachment have been described by Ginn (1999), Ginn et al. (2002), and Johnson et al. (1995).

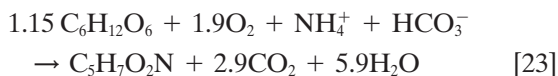
Equations [1] and [4] were solved numerically using implicit, finite-difference approximations. The nonlinearities in Eq. [1] were resolved using a Newton–Raphson iteration method (Brutsaert, 1971). Equation [4] was solved using an alternating split operator approach (Barry et al., 2002; Strang, 1968). Equation [20] and the coupled reaction terms in Eq. [4] were solved using an adaptive time-step Runge–Kutta method (Cash and Karp, 1990). Pressure heads, porosities, and permeabilities were updated at the end of each reaction step to account for biomass-induced changes in fluid-media properties.

Parameter Estimation

The saturated hydraulic conductivity, K_s , of the 40/50 Accusand was determined using the falling head method (Klute, 1986). The water retention characteristics of the clean sand were determined by wet-packing the column, allowing it to drain to a hydrostatic condition, and then sampling each column segment to determine gravimetric water contents. These water contents were then used to calculate volumetric water contents using the overall bulk density of the sand pack. The volumetric water contents were paired with pressure heads for each depth, which were taken as the negative value of the elevation above the location of zero pressure in the hydrostatic column.

The water retention characteristics of the sand were represented using the model of Brooks and Corey (1964). The relative permeability or unsaturated hydraulic conductivity of the sand was represented using the model of Burdine (1953). The hydraulic properties of the attached biomass phase were represented using the models of van Genuchten (1980) and Mualem (1976) with the parameters of a clay soil. The sand and assumed biomass properties were combined using the composite media model described by Rockhold et al. (2002). The hydraulic properties for the sand and biomass are depicted in Fig. 2 and parameter values are given in Table 1.

The parameters in Eq. [19] were estimated from batch growth experiments. The stoichiometry of the biologically mediated redox reaction was estimated using the energetics model of McCarty (1975). This model predicts the following stoichiometry, assuming 60% efficiency in the conversion of glucose to cell biomass ($\text{C}_5\text{H}_7\text{O}_2\text{N}$), with NH_4^+ as the source of N, and with O_2 as the terminal electron acceptor



HK44 is a facultative aerobe capable of denitrification. Therefore a source of NH_4^+ was included in the MMS growth media, rather than NO_3^- , to prevent HK44 from using NO_3^- as an

alternative electron acceptor if anoxic conditions developed. Equation [23] indicates that 1.15 mol of glucose and 1.9 mol of O_2 are required to produce 1 mol of bacterial cells. This translates into $Y_{g/m} = 1.83$ (mg glucose mg^{-1} cells), and $Y_{o/m} = 0.54$ (mg O_2 mg^{-1} cells). Independent batch experiments were also conducted to estimate yield coefficients. The experimentally determined values were variable, but similar to the estimates given by Eq. [23]. Equation [23] was also used to estimate the respiration coefficient, $r_{\text{CO}_2, \text{O}_2} = 1.53$ (mol CO_2 produced mol^{-1} O_2 consumed). Table 1 summarizes the parameters that were used for the base case model simulation.

The initial condition for water flow in the columns was specified as a uniform pressure head, $h(x_i, 0) = 0$ cm (fully saturated). The upper boundary condition was a constant flux, $q_w(0, t) = 7$ cm h^{-1} . The lower boundary condition was specified as a held pressure head that was adjusted in steps to mimic the slow release of water from the columns during the early stages of the experiment, followed by a fixed pressure head of 1 cm at later times. The pressure head steps were: $h(0 \leq t < 0.01) = 43$ cm, $h(0.01 \leq t < 0.02) = 39$ cm, $h(0.02 \leq t < 0.03) = 35$ cm, $h(0.03 \leq t < 0.04) = 30$ cm, $h(0.04 \leq t < 0.05) = 25$ cm, $h(0.05 \leq t < 0.06) = 20$ cm, $h(0.06 \leq t < 0.07) = 15$ cm, $h(0.07 \leq t < 0.08) = 10$ cm, $h(0.08 \leq t < 0.1) = 5$ cm, $h(0.1 \leq t \leq 168) = 1$ cm.

The initial aqueous-phase glucose, O_2 , and CO_2 concentrations were specified as 0.0, 9.2, and 0.01 mg L^{-1} , respectively. These initial O_2 and CO_2 concentrations correspond to equilibrium with gas phase concentrations in the atmosphere as determined using Henry's Law. The upper boundary condition for glucose was a constant concentration of 250 mg L^{-1} . Initial gas-phase concentrations and upper boundary conditions for O_2 and CO_2 were specified to correspond with equilibrium conditions with the atmosphere. The initial aqueous-phase cell concentration was specified as 80.4 mg L^{-1} ($\approx 3 \times 10^8$ CFU mL^{-1}) everywhere, except for the top node in the model grid, where a fixed concentration of 0.0 mg L^{-1} was specified to account for the presence of the UV germicidal lamp, which was turned on at regular intervals during the experiment to prevent cell growth on the surface of the sand. It was further assumed that no bacteria were initially attached to the sand anywhere in the columns.

RESULTS AND DISCUSSION

Increases in pressure heads and water contents were observed during the experiments. One possible mechanism that could cause this behavior is lowering of surface tension due to adsorption of cells and/or biosurfactants at air–water interfaces. Lowering of surface tension would tend to cause desaturation of the porous media, rather than the increases in water content that were observed. Therefore this mechanism may initially seem counter-intuitive. However, localized desaturation would reduce the unsaturated hydraulic conductivity of the porous media, which would effectively increase the resistance to flow, possibly leading to increases in upstream saturations. Independent measurements of surface tension for aqueous solutions of the MMS medium with different concentrations of stationary-phase HK44 cells indicated that surface tension lowering due to sorption of stationary-phase cells alone was not significant (< 1 mN m^{-1}) for cell concentrations up to approximately 10^9 CFU mL^{-1} (Rockhold et al., 2002). However, surface tension was not measured on suspensions of cells that were meta-

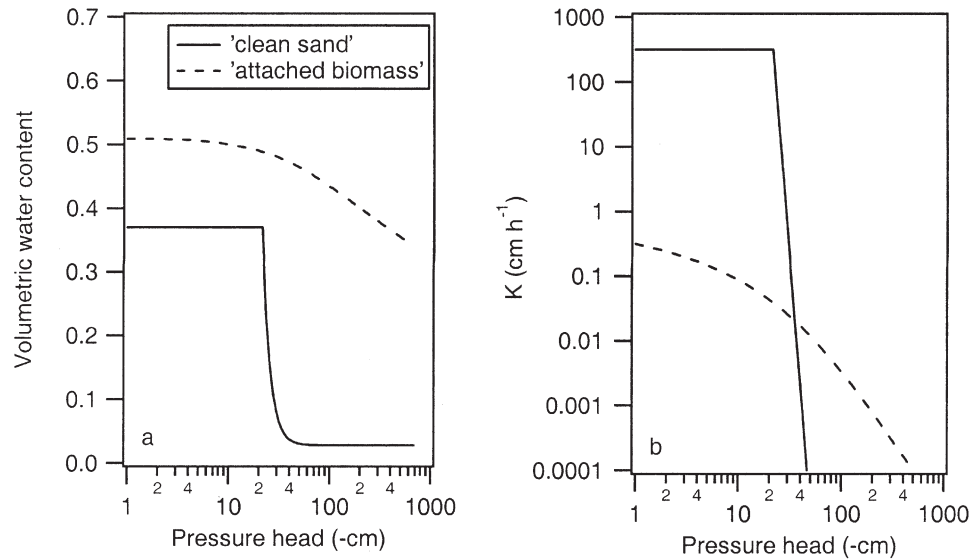


Fig. 2. Hydraulic properties of clean sand and attached biomass phase that were combined using the composite media model described by Rockhold et al. (2002).

bologically active, or under conditions of O_2 stress, or for cell densities $>10^9$ CFU mL^{-1} .

Studies reported by Déziel et al. (1996) and Kosaric (1993) suggest that metabolically active cells may generate surface-active agents and possibly change their surface character to become more hydrophobic. The generation of surface-active compounds (e.g., excess fatty acids) might have resulted in surface tension lowering

in excess of what was observed for stationary-phase cells alone. The anoxic environment that developed during high substrate loading conditions of the experiment might also have promoted the migration of the motile bacteria to air–water interfaces via chemotaxis. Sorption of bacterial cells on the surfaces of mineral grains may also change the wettability of a porous medium, which could result in increases in apparent contact angles (Ab-solom et al., 1983).

Decreases in surface tension and increases in apparent contact angle are both a function of changes in interfacial energies and therefore tend to manifest similar effects. These types of changes were accounted for by similar-media scaling (Rockhold et al., 2002). The apparent surface tension lowering effect was represented by scaling the capillary pressure–saturation curves using scaling factors calculated as

$$\left(\frac{\sigma}{\sigma_0}\right) = 1 - \frac{1}{\sigma_0} A C_{m,w}^B \quad [24]$$

where σ_0 is the surface tension of the cell-free MMS solution (74.2 mN m^{-1}), A and B are empirical parameters, and $C_{m,w}$ is the aqueous-phase cell concentration. Equation [24] is plotted in Fig. 3 using the A and B parameters from Table 1.

Equation [24] was required to approximately reproduce the observed changes in apparent saturations and pressure heads in the columns. It should be noted, however, that capillary pressure represents the difference between the nonwetting (air) and wetting fluid (water) pressures. Therefore if the total gas pressure increases, this could also result in an apparent surface tension lowering effect. The surface tension lowering function serves to capture the effects of possible changes in fluid-media properties, including adsorption of surface-active compounds at gas–liquid interfaces, as well as possible increases in total gas pressure. Changes in total gas pressure due to CO_2 production could be modeled more mechanistically, however, by solving fully coupled equa-

Table 1. Parameters used for model simulations.

Parameter	Base case value (units)	Source or reference
K_s^{sand}	317 (cm h^{-1})	independent measurement
θ_s^{sand}	0.37 ($\text{cm}^3 \text{cm}^{-3}$)	"
θ_0^{sand}	0.028 ($\text{cm}^3 \text{cm}^{-3}$)	"
h_b^{sand}	21.6 (cm)	"
λ^{sand}	5.84	"
K^{biomass}	1.08 (cm h^{-1})	clay soil (Leij et al., 1999)
θ^{biomass}	0.51 ($\text{cm}^3 \text{cm}^{-3}$)	"
$\theta_0^{\text{biomass}}$	0.102 ($\text{cm}^3 \text{cm}^{-3}$)	"
α^{biomass}	0.021 (cm^{-1})	"
n^{biomass}	1.2	"
$b^{\text{composite media}}$	3.17	Clement et al. (1996)
ρ_b	1730 (mg cm^{-3})	independent measurement
ρ_m	1100 (mg cm^{-3})	Bouwer and Rittmann (1992)
α_L	0.5 (cm)	independent measurement
$D_{g,w}^{\text{mol}}$	0.024 ($\text{cm}^2 \text{h}^{-1}$)	Lide (1996)
$D_{O_2}^{\text{mol}}$	0.036 ($\text{cm}^2 \text{h}^{-1}$)	"
$D_{CO_2}^{\text{mol}}$	0.03 ($\text{cm}^2 \text{h}^{-1}$)	"
$D_{m,w}^{\text{mol}}$	0.1 ($\text{cm}^2 \text{h}^{-1}$)	Barton and Ford (1995)
D_{CO_2,N_2}	572.4 ($\text{cm}^2 \text{h}^{-1}$)	Marrero and Mason (1972)
D_{O_2,N_2}	727.2 ($\text{cm}^2 \text{h}^{-1}$)	"
D_{CO_2,CO_2}	572.4 ($\text{cm}^2 \text{h}^{-1}$)	"
$K_{H_2O_2}$	43.8 [(L atm) (mol K^{-1})]	Sawyer et al. (1994)
$K_{H_2CO_2}$	29.5 [(L atm) (mol K^{-1})]	"
a	2.42	fit to experimental data
e	1	Moldrup et al. (2000)
A	60	fit to experimental data
B	0.54	"
σ_0	74.2 (mN m^{-1})	independent measurement
μ_{max}	0.496 (h^{-1})	"
K_g	10.7 (mg L^{-1})	"
K_o	1.5 (mg L^{-1})	fit to experimental data
$Y_{g/m}^{\text{mol}}$	1.83 (mg mg^{-1})	Eq. [23]
$Y_{o/m}$	0.54 (mg mg^{-1})	"
$Y_{c/m}$	1.13 (mg mg^{-1})	"
R	1.53 ($\text{mol CO}_2 \text{mol}^{-1} O_2$)	"
α_c	0.1	fit to experimental data
f	0.29 (h^{-1})	"
g	0.014 (h^{-1})	"

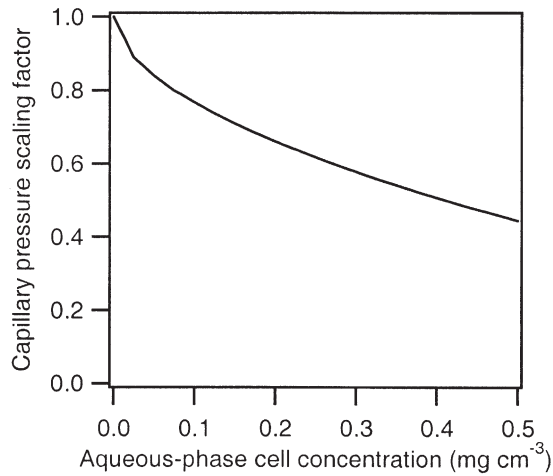


Fig. 3. Capillary pressure scaling function.

tions for the flow of both water and air, with source terms in the air equation to account for possible gas pressure buildup.

Figure 4 shows time histories of observed and simulated effluent glucose, O₂, and biomass concentrations, and the final sand-associated biomass concentration distributions for the columns. The error bars in Fig. 4 repre-

sent standard deviations of three analytical repetitions. The simulation results match the observed effluent glucose and biomass concentration data reasonably well. However, the DO data indicate relatively constant concentrations of approximately 1 mg L⁻¹ in the effluent after the initial drainage period, whereas the simulation results indicate that the concentration of DO in the effluent at these times was near zero. Differences between observed and simulated effluent DO concentrations may be due to (i) partial re-oxygenation of the effluent DO samples as they were transferred from the sampling syringes on the columns to the measurement vessel, (ii) diminished HK44 respiration rates at low DO concentrations that were not accounted for in the model, and/or (iii) gas-liquid mass transfer limitations associated with adsorption of cells and/or biosurfactants at gas-liquid interfaces.

The equilibrium concentration of O₂ in deionized water at atmospheric pressure with a partial O₂ gas pressure of 0.021 MPa (0.21 atm) is 9.2 mg L⁻¹ (Lide, 1996). The stoichiometry indicated by Eq. [23] suggests that for this DO concentration, only about 31 of the 250 mg L⁻¹ of glucose in the influent would be consumed, leaving a concentration of 219 mg L⁻¹ glucose in the column effluent. Simulations that neglected gas diffusion verified this

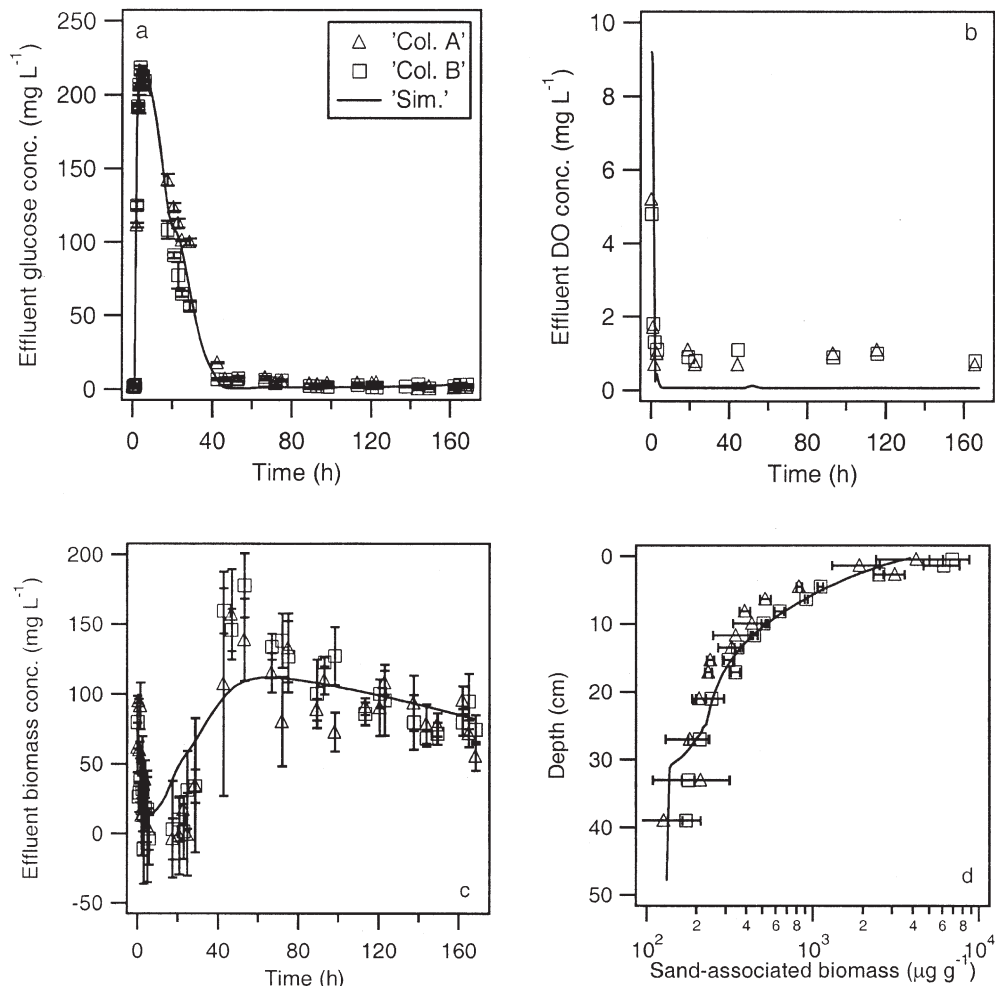


Fig. 4. Observed and simulated effluent glucose, dissolved oxygen, and biomass concentrations, and final, sand-associated (attached) biomass distributions.

calculation. However, gas diffusion results in O_2 being replenished at a much faster rate than is possible by advection and diffusion in the aqueous phase alone, thus allowing virtually all of the glucose to be utilized. This result demonstrates the importance of gas-phase diffusion to soil respiration.

The gradual decrease in effluent biomass concentrations that was observed after about 60 h (Fig. 4) required the use of a time-dependent detachment rate coefficient (Eq. [22]) to reproduce this behavior in the model simulations. However, this effect might also have been achieved by accounting for biomass decay or cell death. Decreases in effluent biomass concentrations might also have been due, at least in part, to decreases in the effective growth rate of the bacteria, possibly resulting from gas-liquid or liquid-cell mass transfer limitations that developed with time (Rockhold et al., 2004). For example, Bailey and Ollis (1986) noted that for a variety of sparingly soluble gases, surfactant adsorption at gas-liquid interfaces resulted in an average reduction in the interphase mass transfer coefficient of 60%. The observed and simulated results shown in Fig. 4 deviate somewhat between times of about 5 and 50 h, with the observed effluent data exhibiting lower concentrations than the simulation results between 5 and 30 h, and higher concentrations than the simulation results between 40 and 50 h. These differences may be attributable

to other phenomena such as irreversible sorption of bacteria on Fe oxide coatings on the sand and/or on air-water interfaces.

Figure 4 also shows the observed and simulated final sand-associated biomass concentration distributions in the columns. The apparently abrupt increase in attached cell concentrations indicated by the simulation results at a depth of approximately 30 cm reflects the position of the capillary fringe. Below a depth of about 32 cm, the sand is fully water saturated, with a volumetric water content, $\theta_w \approx 0.37$. Water contents decrease rapidly above this depth, and at the 27-cm depth $\theta_w \approx 0.15$. In the upper, unsaturated part of the columns, ample O_2 supply, which is replenished by gas-phase diffusion, allows for more cell growth relative to the lower saturated parts of the columns. The attachment coefficient, k_i , also increases as water content decreases, as indicated by Eq. [21].

Figure 5 shows time histories of observed and simulated values of volumetric water content and pressure head at selected locations. The observed changes in water contents and pressures could only be reproduced approximately in the model simulations by using fluid-media scaling to account for an apparent surface-tension lowering effect. As shown in Fig. 6, significant increases in apparent volumetric water contents were only observed at the uppermost TDR measurement locations, approxi-

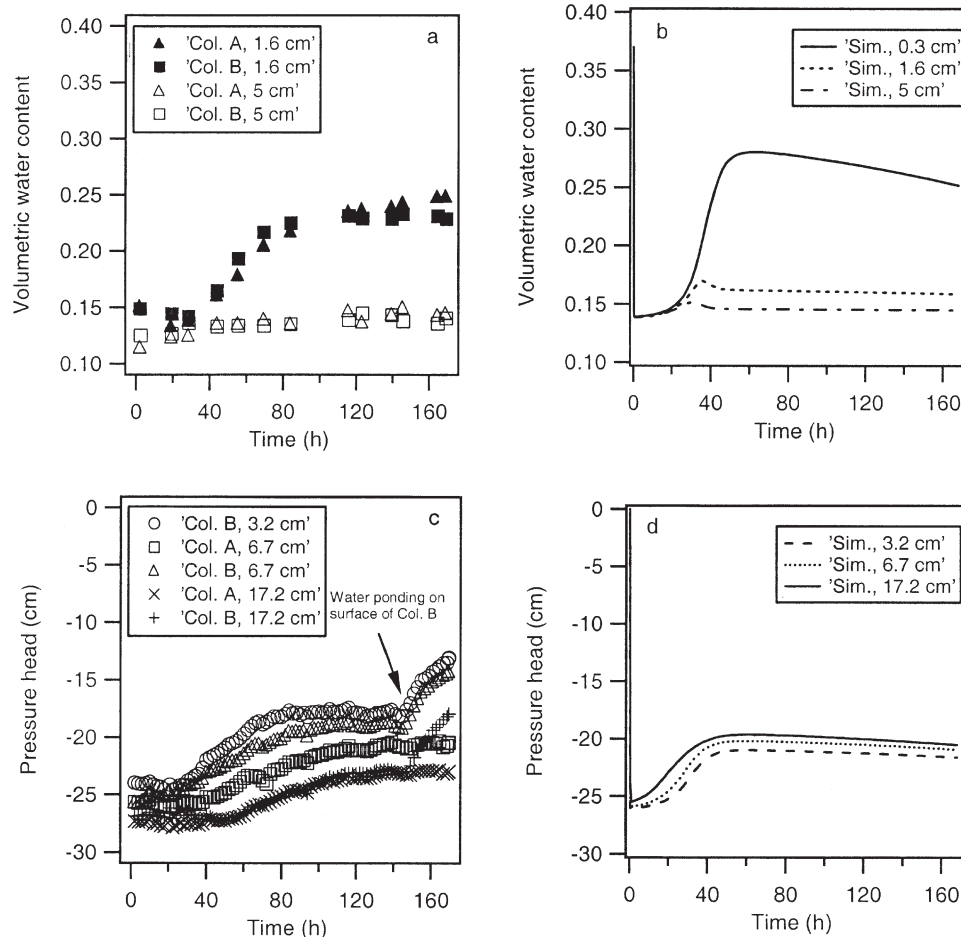


Fig. 5. Observed and simulated time histories of water content and pressure heads at selected depths.

mately 1.6 cm below the surface of the sand in the columns. The simulated water contents shown in Fig. 5 indicate relatively small increases in volumetric water contents at depths of 1.6 cm and below. However, significant increases in water content are predicted for the uppermost node in the model grid, located at a depth of approximately 0.3 cm. The differences between the observed and simulated water contents may be due, in part, to the larger measurement volumes sensed by the TDR probes.

Water content measurement by TDR is a function of the dielectric permittivities of the materials in which the probes (or waveguides) are embedded (e.g., water, air, sand, and biomass). The energy of the electromagnetic (EM) pulse that is propagated and reflected back during a measurement is most highly concentrated in the immediate vicinity of the waveguides, and decreases rapidly with distance away from them (Knight, 1992). At higher water contents, the energy of the EM pulse would not propagate as far away from the waveguides because of the higher dielectric permittivity of water (≈ 80) relative to air (≈ 1). It is possible that the uppermost TDR measurements were influenced by the accumulation of biomass. Bacterial cells are typically on the order of 70 to 90% water by volume (Madigan et al., 1997). Therefore they might be expected to appear similar to water in terms of an apparent water content measured by TDR. However, the molecular structure of bacterial cells is certainly different than water and would have different relaxation frequencies. The TDR measurements may be susceptible to bias of this type due to the high bandwidth of the Tektronix Model 11801 oscilloscope. The volumes sampled by the TDR measurements at the 1.6-cm depth may extend up to the surface of the sand in the columns and become progressively more biased with time because of the higher biomass concentrations that develop

near the surface. The possible influence of bacterial cell accumulation on TDR measurements was not investigated or accounted for in the TDR probe calibrations.

Figure 5 also shows time histories of observed and simulated pressure head values, respectively, at selected measurement depths. Two of the tensiometer segments in Column A developed air leaks that rendered the data from those locations useless. Unlike the TDR data, which showed significant increases in apparent volumetric water contents only near the surface, the transducer data indicate significant increases in pressure heads at all depths. A steady water flux was established on the surfaces of the columns. Therefore differences between measured values of pressure heads at different depths that should all be under a unit hydraulic gradient may be indicative of nonuniformities in packing and/or bacterial-induced changes in the hydraulic properties of the sand.

The transducer data for Column B show sudden increases in the rates of change of pressure heads at a time of approximately 145 h. These increases in pressure head correspond with the start of ponding of the influent on the surface of Column B that occurred at this time, as noted in Fig. 5. At this point, the hydraulic conductivity of the sand in Column B was reduced from its original saturated value of approximately 317 cm h^{-1} to $<7 \text{ cm h}^{-1}$, which represents a 45-fold decrease. Ponded water at the surface effectively reduces the air permeability to zero, preventing gas from either entering or exiting the column. The sudden rate of increase in pressure heads after 145 h is due to compression of gas trapped below the ponded water while infiltration continued, as well as possible gas pressure buildup due to the continued production of CO_2 by bacteria within the column. After 145 h, the single-phase Richards equation is clearly no longer valid for modeling these systems.

The calculated partial pressures of O_2 and CO_2 in the columns at the top of the capillary fringe ($\approx 30 \text{ cm}$ depth) just before destructive sampling (168 h) were approximately 0.0001 and 0.035 MPa (0.001 and 0.35 atm), respectively. In order for atmospheric pressure to be maintained in this system, the increase in the partial pressure of CO_2 above 0.021 MPa would require the partial pressure of N_2 to decrease from about 0.079 to 0.065 MPa. If N_2 is more or less stagnant, nonequimolar respiration ($r > 1$) would tend to increase the total gas pressure in the system as a result of excess production of CO_2 . If the upper boundary of the system is maintained at atmospheric pressure, even very slight increases in total gas pressure within the columns would lead to some advective movement of gases out of the system, rather than just the simple Fickian diffusion process that was represented in the model (Lefelaar, 1988; Freijer and Lefelaar, 1996). Total gas pressures would tend to adjust so that they remain close to atmospheric pressure, as long as the gas phase is continuous throughout the porous media, and resistance to air flow is negligible. Additional considerations for modeling gas transport in unsaturated porous media are discussed by Thorstenson and Pollock (1989).

Figure 6 shows the measured water retention characteristics and fitted Brooks–Corey model representing

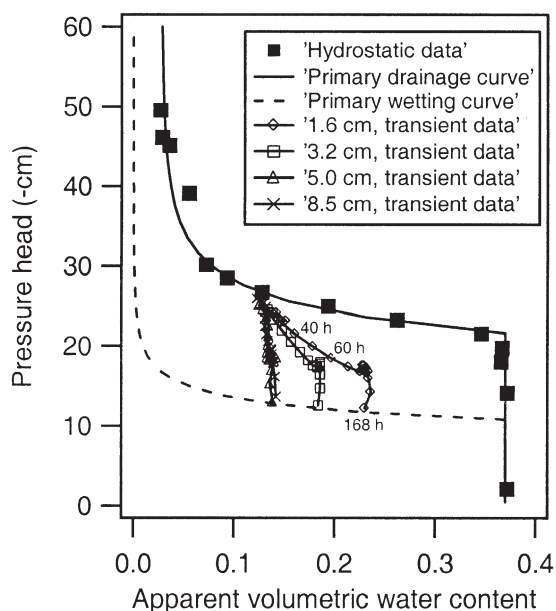


Fig. 6. Water retention data with Brooks–Corey (1964) model fit for clean sand, and data measured from tensiometers and TDR probes during the column experiment.

the primary drainage curve for the clean 40/50 Accusand, and pressure-saturation values from various depths in Column B that were calculated from the transducer and TDR data during the experiment. Also shown in Fig. 6 is a hypothetical wetting curve resulting from simple scaling of the drainage curve, using an assumed contact angle of 30°. It is not known whether the apparent changes in water content and pressure heads that were observed in these experiments resulted primarily from (i) clogging of pore throats by cell aggregates or biofilms, (ii) CO₂ gas generation and occlusion, (iii) production of biosurfactants (e.g., excess fatty acid production due to the high substrate loading conditions) with concomitant lowering of gas-liquid interfacial tension, (iv) changes in the wettability of the sand as it became coated by biofilms, or (v) a combination of these factors. A combination of these factors is most likely. Regardless of the mechanism(s), it is clear from these experiments that biomass-induced changes in the hydraulic properties of variably saturated porous media can be significant. Such changes are not typically considered when modeling flow and reactive transport processes in soils.

SUMMARY AND CONCLUSIONS

An experimental and numerical investigation was conducted to study interactions between microbial dynamics and transport processes in sand-packed columns under initially steady, variably saturated flow conditions. Glucose was used as the sole C source for growth of *Pseudomonas fluorescens* HK44. Increases in pressure heads were observed at all measured depths during the experiment, but significant increases in apparent volumetric water contents only occurred within the upper 5 cm of the columns, corresponding to the areas of highest attached biomass concentrations. The hydraulic conductivity of the sand was reduced by a factor of 45 during the 1-wk experiment. To the best of our knowledge, this is one of the first experiments to document bacterially induced changes in the hydraulic properties of unsaturated porous media during active cell growth and transport.

The experiment was simulated using the single-phase Richards equation to model water flow and advection-dispersion reaction reactions to model solute and bacterial transport, cell growth and accumulation, glucose and O₂ consumption, and gas diffusion and exchange. Reasonably good matches were obtained between observed and simulated effluent glucose and biomass data and final sand-associated (attached) biomass concentration distributions using first-order reversible attachment-detachment kinetics with attachment coefficients based on particle-filtration theory, and time-dependent detachment rate coefficients. The observed changes in water contents and pressure heads were reproduced approximately using fluid-media scaling to account for an apparent surface-tension lowering effect.

During the experiment, ponded water developed on the surface of one of the columns after about 6 d. Pressure head readings increased rapidly after this time, while water contents remained relatively constant, indicating

compression of entrapped gas and possible buildup of gas pressure due to continued production of CO₂ by bacteria. The single-phase Richards equation was no longer valid for modeling the experiment after this point because the air phase was discontinuous.

These results illustrate the potential importance of using fully coupled multifluid flow equations, rather than the single-phase Richards equation, and multicomponent reactive transport equations to model coupled biogeochemical reactions and transport in soils.

Considerable uncertainties remain as to the exact mechanism(s) responsible for the changes in hydraulic properties that were observed during this study, suggesting that further experimental work is warranted. Using additional instrumentation such as microelectrodes, (DeBeer and Schramm, 1999; Lewandowski et al., 1999) and in-line gas sampling, might allow a more complete understanding of the mechanisms and process interactions.

REFERENCES

- Absolom, D.R., F.V. Lamberti, Z. Policova, W. Zingg, C.J. van Oss, and A.W. Neumann. 1983. Surface thermodynamics of bacterial adhesion. *Appl. Environ. Microbiol.* 46:90-97.
- Allen-King, R.M., R.W. Gillham, and J.F. Barker. 1996a. Fate of dissolved toluene during steady infiltration through unsaturated soil: I. Method emphasizing chloroform as a volatile, sorptive, and recalcitrant tracer. *J. Environ. Qual.* 25:279-286.
- Allen-King, R.M., R.W. Gillham, J.F. Barker, and E.A. Sudicky. 1996b. Fate of dissolved toluene during steady infiltration through unsaturated soil: II. Biotransformation under nutrient-limited conditions. *J. Environ. Qual.* 25:287-295.
- Bailey, J.E., and D.F. Ollis. 1986. *Biochemical engineering fundamentals*. McGraw-Hill, New York.
- Barry, D.A., H. Prommer, C.T. Miller, P. Engesgaard, A. Brun, and C. Zheng. 2002. Modelling the fate of oxidisable organic contaminants in groundwater. *Adv. Water Resour.* 25:945-983.
- Barton, J.W., and R.M. Ford. 1995. Determination of effective transport coefficients for bacterial migration in sand columns. *Appl. Environ. Microbiol.* 61:3329-3335.
- Bouwer, E.J., and B.E. Rittmann. 1992. Comment on: Use of colloid filtration theory for modeling movement of bacteria through a contaminated sandy aquifer. *Environ. Sci. Technol.* 26:400-401.
- Brink, R.H., P. Dubach, and D.L. Lynch. 1960. Measurement of carbohydrates in soil hydrolyzates with anthrone. *Soil Sci.* 89:157-166.
- Brooks, R.H., and A.T. Corey. 1964. Hydraulic properties of porous media. *Hydrol. Paper 3*. Colorado State University, Fort Collins.
- Brutsaert, W.F. 1971. A functional iteration technique for solving the Richards equation applied to two-dimensional infiltration problems. *Water Resour. Res.* 7:1583-1596.
- Burdine, N.T. 1953. Relative permeability calculations from size distribution data. *Trans. Am. Inst. Mining Metall. Pet. Eng.* 198:71-77.
- Cash, J.R., and A.H. Karp. 1990. A variable order Runge-Kutta method for initial value problems with rapidly varying right-hand sides. *ACM Trans. Math. Soft.* 16:201-222.
- Clement, T.P., B.S. Hooker, and R.S. Skeen. 1996. Macroscopic models for predicting changes in saturated porous media properties caused by microbial growth. *Ground Water* 34:934-942.
- De Beer, D., and A. Schramm. 1999. Micro-environments and mass transfer phenomena in biofilms studied with micro-sensors. *Water Sci. Technol.* 7:173-178.
- Deshpande, P.A., and D.R. Shonnard. 1999. Modeling the effects of systematic variation in ionic strength on the attachment kinetics of *Pseudomonas fluorescens* UPER-1 in saturated sand columns. *Water Resour. Res.* 5:1619-1627.
- Déziel, E., G. Paquette, R. Villemur, F. Lepine, and J. Bisailon. 1996. Biosurfactant production by a soil *Pseudomonas* strain growing on polycyclic aromatic hydrocarbons. *Appl. Environ. Microbiol.* 62:1908-1912.
- Estrella, M.R., M.L. Brusseau, R.S. Maier, I.L. Pepper, P.J. Wierenga,

- and R.M. Miller. 1993. Biodegradation, sorption, and transport of 2,4-D acid in saturated and unsaturated soils. *Appl. Environ. Microbiol.* 59:4266–4273.
- Freijer, J.I., and P.A. Leffelaar. 1996. Adapted Fick's law applied to soil respiration. *Water Resour. Res.* 32:791–800.
- Ginn, T.R. 1999. On the distribution of multi-component mixtures over generalized exposure time in subsurface flow and reactive transport: Foundations and formulations for groundwater age, chemical heterogeneity, and biodegradation. *Water Resour. Res.* 35:1395–1407.
- Ginn, T.R., B.D. Wood, K.E. Nelson, T.D. Scheibe, E.M. Murphy, and T.P. Clement. 2002. Processes in microbial transport in the natural subsurface. *Adv. Water Resour.* 25:1017–1042.
- Jaynes, D.B., and A.S. Rogowski. 1983. Applicability of Fick's law to gas diffusion. *Soil Sci. Soc. Am. J.* 47:425–430.
- Jewett, D.G., B.E. Logan, R.G. Arnold, and R.C. Bales. 1999. Transport of *Pseudomonas fluorescens* through quartz sand columns as a function of water content. *J. Contam. Hydrol.* 36:73–89.
- Johnson, W.P., K.A. Blue, B.E. Logan, and R.G. Arnold. 1995. Modeling bacterial detachment during transport as a residence-time-dependent process. *Water Resour. Res.* 31:2649–2658.
- Kelly, S.F., J.S. Selker, and J.L. Green. 1995. Using short soil moisture probes with high-bandwidth time-domain-reflectometry instruments. *Soil Sci. Soc. Am. J.* 59:97–102.
- King, J.M.H., P.M. DiGrazia, B.M. Applegate, R.S. Burlage, J. Sanseverino, P. Dunbar, F. Larimer, and G.S. Saylor. 1990. Rapid, sensitive bioluminescent reporter technology for naphthalene exposure and biodegradation. *Science (Washington, DC)* 249:778–781.
- Klute, A. (ed.) 1986. *Methods of soil analysis*. Agron. Monogr. 9. ASA and SSSA, Madison, WI.
- Knight, J.H. 1992. Sensitivity of time domain reflectometry measurements to lateral variations in soil water content. *Water Resour. Res.* 28:2345–2352.
- Kosaric, N. (ed.) 1993. *Biosurfactants*. Marcel Dekker, New York.
- Langner, H.W., W.P. Inskeep, H.M. Gaber, W.L. Jones, D.S. Das, and J.M. Wraith. 1998. Pore water velocity and residence time effects on the degradation of 2,4-D during transport. *Environ. Sci. Technol.* 32:1308–1315.
- Lee, W.-K., J. McGuire, and M.K. Bothwell. 1999. A mechanistic approach to modeling protein adsorption at solid-water interfaces. *J. Colloid Interface Sci.* 213:265–267.
- Leffelaar, P.A. 1988. Dynamics of partial anaerobiosis, denitrification, and water in a soil aggregate: Simulation. *Soil Sci.* 146:427–444.
- Leij, F.J., W.J. Alves, and M.Th. van Genuchten. 1999. The UNSODA Unsaturated Soil Hydraulic Database. p. 1269–1281. *In* van Genuchten et al. (ed.) *Characterization and measurement of the hydraulic properties of unsaturated porous media*. Part 2. University of California Press, Riverside.
- Lewandowski, Z., D. Webb, M. Hamilton, and G. Harkin. 1999. Quantifying biofilm structure. *Water Sci. Technol.* 39:71–76.
- Lide, D.R. (ed.) 1996. *Handbook of chemistry and physics*. CRC Press, Boca Raton, FL.
- Logan, B.E., D.G. Jewett, R.G. Arnold, E.J. Bouwer, and C.R. O'Melia. 1995. Clarification of clean-bed filtration models. *J. Environ. Eng.* 121:869–873.
- Madigan, M.T., J.M. Martinko, and J. Parker. 1997. *Brock Biology of Microorganisms*. Prentice Hall, Upper Saddle River, NJ.
- Marrero, T.R., and E.A. Mason. 1972. Gaseous diffusion coefficients. *J. Phys. Chem. Ref. Data.* 1:3–118.
- McCarty, P.L. 1975. Stoichiometry of biological reactions. *Prog. Water Technol.* 7:157–172.
- Megee, R.D., III, S. Kinoshita, A.G. Fredrickson, and H.M. Tsuchiya. 1970. Differentiation and product formation in molds. *Biotech. Bioeng.* 12:771–801.
- Millington, R.J., and J.M. Quirk. 1961. Permeability of porous solids. *Trans. Faraday Soc.* 57:1200–1207.
- Moldrup, P., T. Olesen, J. Gamst, P. Schjønning, T. Yamaguchi, and D.E. Rolston. 2000. Predicting the gas diffusion coefficient in re-packed soil: Water-induced linear reduction model. *Soil Sci. Soc. Am. J.* 64:1588–1594.
- Mualem, Y. 1976. A new model for predicting the hydraulic conductivity of unsaturated porous media. *Water Resour. Res.* 12:513–522.
- Powelson, D.K., and A.L. Mills. 1998. Water saturation and surfactant effects on bacterial transport in sand columns. *Soil Sci.* 163:694–704.
- Rajagopalan, R., and C. Tien. 1976. Trajectory analysis of deep-bed filtration with the sphere-in-cell porous media model. *AIChE J.* 3:523–533.
- Richards, L.A. 1931. Capillary conduction of liquids through porous mediums. *Physics* 1:318–333.
- Rockhold, M.L., R.R. Yarwood, M.R. Niemet, P.J. Bottomley, and J.S. Selker. 2002. Considerations for modeling bacterial-induced changes in hydraulic properties of variably saturated porous media. *Adv. Water Resour.* 25:477–495.
- Rockhold, M.L., R.R. Yarwood, and J.S. Selker. 2004. Coupled microbial and transport processes in soils. Available at www.vadosezonejournal.org. *Vadose Zone J.* 3:368–383.
- Sawyer, C.N., P.L. McCarty, and G.F. Parkin. 1994. *Chemistry for environmental engineering*. McGraw-Hill, New York.
- Schäfer, A., P. Ustohal, H. Harms, F. Stauffer, T. Dracos, and A.J.B. Zehnder. 1998. Transport of bacteria in unsaturated porous media. *J. Contam. Hydrol.* 33:149–169.
- Schroth, M.H., S.J. Ahearn, J.S. Selker, and J.D. Istok. 1996. Characterization of Miller-similar sands for laboratory hydrologic studies. *Soil Sci. Soc. Am. J.* 60:1331–1339.
- Šimunek, J., and D.L. Suarez. 1993. Modeling of carbon dioxide transport and production in soil. 1. Model development. *Water Resour. Res.* 29:487–497.
- Smith, P.K., R.I. Krohn, G.T. Hermanson, A.K. Mallia, F.H. Gartner, M.D. Provenzano, E.K. Fujimoto, N.M. Goeke, B.J. Olson, and D.C. Klenk. 1985. Measurement of protein using bicinchoninic acid. *Anal. Biochem.* 150:76–85.
- Strang, G. 1968. On the construction and comparison of difference schemes. *SIAM J. Numer. Anal.* 5:506–517.
- Tan, Y.W., J. Bond, and D.M. Griffin. 1992. Transport of bacteria during unsteady unsaturated soil water flow. *Soil Sci. Soc. Am. J.* 56:1331–1340.
- Thorntson, D.C., and D.P. Pollock. 1989. Gas transport in unsaturated zones: Multicomponent systems and the adequacy of Fick's law. *Water Resour. Res.* 25:477–507.
- Tien, C., R.M. Turian, and H. Pendse. 1979. Simulation of the dynamic behavior of deep bed filters. *AIChE J.* 3:385–395.
- van Genuchten, M.Th. 1980. A closed-form equation for predicting the hydraulic conductivity of unsaturated soils. *Soil Sci. Soc. Am. J.* 44:892–898.
- Wan, J., J.L. Wilson, and T.L. Kieft. 1994. Influence of gas-water interface on transport of microorganisms through unsaturated porous media. *Appl. Environ. Microbiol.* 60:509–516.
- Yarwood, R.R., M.L. Rockhold, M.R. Niemet, J.S. Selker, and P.J. Bottomley. 2002. Bioluminescence as a nondestructive measure of microbial cell density and distribution in unsaturated porous media. *Appl. Environ. Microbiol.* 68:3597–3605.